Naval Research Laboratory
Stennis Space Center, MS 39529-5004
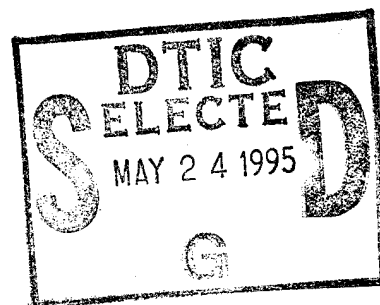
Applications of Sector-Focusing Processing for Stabilized Matched-Field Localization in Shallow Water

CHRISTOPHER FEUILLADE
HOWARD A. CHANDLER
GEORGE B. SMITH

Ocean Acoustics Branch
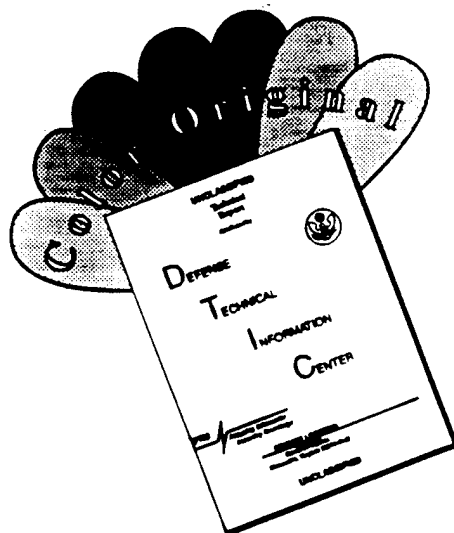*Center for Environmental Acoustics*

DTIC
SELECTED
MAY 2 4 1995
G

April 19, 1995

19950519 042

DTIC QUALITY INSPECTED 5

DISCLAIMER NOTICE

THIS DOCUMENT IS BEST QUALITY AVAILABLE. THE COPY FURNISHED TO DTIC CONTAINED A SIGNIFICANT NUMBER OF COLOR PAGES WHICH DO NOT REPRODUCE LEGIBLY ON BLACK AND WHITE MICROFICHE.

REPORT DOCUMENTATION PAGE

Form Approved
OBM No. 0704-0188

Public reporting burden for this collection of information is estimated to average 1 hour per response, including the time for reviewing instructions, searching existing data sources, gathering and maintaining the data needed, and completing and reviewing the collection of information. Send comments regarding this burden or any other aspect of this collection of information, including suggestions for reducing this burden, to Washington Headquarters Services, Directorate for information Operations and Reports, 1215 Jefferson Davis Highway, Suite 1204, Arlington, VA 22202-4302, and to the Office of Management and Budget, Paperwork Reduction Project (0704-0188), Washington, DC 20503.

1. AGENCY USE ONLY *(Leave blank)*	2. REPORT DATE April 19, 1995	3. REPORT TYPE AND DATES COVERED Final

4. TITLE AND SUBTITLE

Applications of Sector-Focusing Processing for Stabilized Matched-Field Localization in Shallow Water

6. AUTHOR(S)

Christopher Feuillade, Howard A. Chandler, and George B. Smith

5. FUNDING NUMBERS

Job Order No.	571505803
Program Element No.	0601153N
Project No.	03202
Task No.	350
Accession No.	DN255005

7. PERFORMING ORGANIZATION NAME(S) AND ADDRESS(ES)

Naval Research Laboratory
Center for Environmental Acoustics
Stennis Space Center, MS 39529-5004

8. PERFORMING ORGANIZATION REPORT NUMBER

NRL/FR/7173--93-9445

9. SPONSORING/MONITORING AGENCY NAME(S) AND ADDRESS(ES)

10. SPONSORING/MONITORING AGENCY REPORT NUMBER

11. SUPPLEMENTARY NOTES

12a. DISTRIBUTION/AVAILABILITY STATEMENT

Approved for public release; distribution unlimited.

12b. DISTRIBUTION CODE

13. ABSTRACT *(Maximum 200 words)*

The sector-focusing (SF) method has been introduced as a technique for performing high-resolution acoustic matched-field processing in a waveguide. The SF methodology is highly effective against sensor phase error and geoacoustic mismatch in an environment dominated by modal noise. Sector focusing is a readily adaptable signal processing technique in that specific implementation strategies may be designed for application to individual environmental situations. In this report, the mathematical framework for SF is explored, and the mechanisms of mismatch induced instability described. The technique is then developed to demonstrate how the wide range of parameter options available for its implementation (i.e., variable sector size, shape, and dimensionality) provide flexibility to achieve stabilized localization performance for a broad range of conditions.

Using the example of a continuous wave source in a noisy shallow-water channel, the SACLANTCEN Normal-Mode Acoustic Propagation (SNAP) model was used to generate replica acoustic pressure fields for the water channel with a depth variable sound speed profile. SNAP was also used to simulate a "detected" field due to an acoustic source in the presence of modal noise. These fields were then correlated using SF, which was applied via a "sliding" sector algorithm. The sector parameters were adjusted to optimize peak localization and to eliminate instabilities when mismatch was introduced. It was found that SF can always be made to achieve the stability of the Bartlett processor in the "small" sector limit. In the "large" sector limit, SF is seen to be equivalent to the reduced maximum likelihood processor.

14. SUBJECT TERMS

shallow water, algorithms, matched field

15. NUMBER OF PAGES
23

16. PRICE CODE

17. SECURITY CLASSIFICATION OF REPORT	18. SECURITY CLASSIFICATION OF THIS PAGE	19. SECURITY CLASSIFICATION OF ABSTRACT	20. LIMITATION OF ABSTRACT
Unclassified	Unclassified	Unclassified	Same as report

CONTENTS

ii

APPLICATIONS OF SECTOR-FOCUSING PROCESSING FOR STABILIZED MATCHED-FIELD LOCALIZATION IN SHALLOW WATER

1.0 INTRODUCTION

Since it was first discussed by Bucker and others almost 20 years ago [1–3], matched-field processing (MFP) notably increased in popularity as a technique for performing underwater acoustic array processing in a waveguide environment, where plane-wave signal vector assumptions do not apply. The typical MFP procedure is to compare (or "match") the signal replica vectors obtained from a model of the acoustic propagation, using a series of trial source locations, with vectors derived from received signal data. When the trial source location and the true source location correspond, the two vectors should be highly correlated. The method has been successfully applied to continuous wave signals from a few hertz to several kilohertz.

Much initial work in MFP consisted of the development and assessment of various algorithms for matching the two sets of signals. Heitmeyer et al. [4] discussed MFP in a Pekeris channel, using a simple normalized cross-correlation of the two vectors. This commonly used method is now generally referred to as the "conventional" or "Bartlett" processor: the latter term acknowledges its roots in the signal processing literature [5]. Another broad group of techniques, typically used for waveguide scenarios and acoustic frequencies where the number of modes is less than the number of receivers, is encompassed by the term "mode space processing." Here, a matrix transformation is performed to obtain reduced vectors of modal amplitude coefficients from the replica and data signal vectors [6]. These can be cross-correlated using a direct equivalent of the Bartlett method, or otherwise processed using such high-resolution techniques as the "reduced maximum likelihood" (RML) processor, which we shall describe later. In the mode space context, Shang et al. [7–9] studied range and depth estimation as separable problems. Yang [10–13] also investigated modal decomposition and mode filtering methods for improving source localization. Wilson et al. [14] considered the application of mode filtering to the case where the number of modes is greater than the number of receivers.

Although the Bartlett method of range-depth estimation has been widely used, it frequently produces unsatisfactory ambiguity surfaces with broad source peaks and high sidelobes, which closely resemble and compete with the source peak. To obtain smoother and more interpretable surfaces, attention has turned to the use of nonlinear high-resolution processors. The most extensively studied is Capon's estimator [15], which is also known as the "maximum likelihood" (ML) method [16] and the "minimum variance distortionless response" [17]. The ML processor has been successfully applied to the analysis of shallow- [18] and deep-water [19] experiments.

It is widely recognized that ML is very sensitive to mismatch between the model used to calculate the replica field and the actual data. The mismatch may be due to inaccurate or incomplete knowledge of the requisite environmental parameters, or to system effects. Much recent work has

1

been concerned with studying the nature and magnitude of the mismatch problem under various scenarios, both for MFP in general [20–24], and for the ML processor in particular [25–29].

Mismatch is probably the most significant obstacle to the general experimental application of MFP techniques. The sensitivity of MFP to system or environmental modeling errors is due to the fact that, to be successfully implemented, it requires the full structure of the complex acoustic field in the waveguide. ML behaves very satisfactorily, typically giving sharp, narrow signal peaks discriminated against a low, flat background when the mismatch is slight. Its performance deteriorates sharply with only relatively minor degrees of mismatch, however, and interest has necessarily grown in the development of more robust high-resolution methods that will continue to give stable estimates even in the presence of mismatch. One approach is that adopted by Baggeroer et al. [30] and Schmidt et al. [31], who recently introduced the multiple constraint beamformer (MCM). This method, which may be seen as a generalization of ML, attempts to overcome mismatch-induced instabilities by increasing the single point look constraint of ML through the introduction of several additional constraints around the look direction. Their most successful processing with this method was obtained [30,31] by designing the constraint conditions to achieve Bartlett behavior in the neighborhood of the source peak, but ML behavior over the search region as a whole—an approach that combines the stability of the Bartlett estimator with the background-reducing characteristics of ML.

The method of sector-focused (SF) MFP used for eliminating mismatch instabilities represents an essentially different signal processing philosophy from the MCM approach outlined above. MCM recognizes that mismatch will lead to uncertainties in the location and size of the source peak and attempts to improve the chances of finding it by increasing the physical aperture of the processor "probe." SF, however, seeks to remove the effects of mismatch by eliminating degrees of freedom from the cross-spectral matrix (CSM) that contain no signal information, but do contribute to the instability. Byrne and Steele [32] showed, in a plane-wave beamforming context, that some eigenvectors of the CSM become unstable in the presence of correlated noise, causing ML to deteriorate with mismatch. They subsequently introduced SF to stabilize ML in the plane-wave case [33]. Byrne et al. [34] applied the SF approach to the case of normal mode propagation in a waveguide. The resulting algorithm, RML, is particularly effective when the number of modes is significantly less than the number of receivers, and shows much improved stability to phase errors (as a type of system mismatch) in the presence of correlated noise. Frichter et al. [35] extended this application and demonstrated a general implementation of SF in a deeper waveguide with small spatial sectors. Smith et al. [36] showed that SF could also be effectively implemented to stabilize MFP against environmental modeling errors by successfully localizing a source in a shallow-water waveguide with a highly mismatched, downward-refracting sound speed profile.

Sector focusing is a powerful and flexible signal processing technique. Both the size and shape of the sector are variable. Once these quantities have been chosen, the dimensionality of the projection matrix derived from the sector can also be selectively adjusted. These three parameters together provide a wide variety of options for maximizing the performance of the technique, which is particularly useful for resolving multiple sources in a highly mismatched environment [37].

We present an elaboration of the derivation of the SF algorithm presented in reference [35] that clearly indicates where the mechanisms of mismatch-induced instability lie within ML. We then show how these may be avoided by eliminating degrees of freedom from the CSM. Then, using the example of a continuous wave source in a shallow-water channel, we demonstrate how sector size, shape, and dimensionality can be adjusted to suit the physical characteristics of the waveguide, and to take best advantage of the SF dimensionality reduction procedure to stabilize the localization

process. We also explain the relationship of SF to the Bartlett and RML processors, in the small and large sector limits, respectively. Our overall purpose is to take a significant step toward a comprehensive appreciation of the method and to provide a helpful guide to its successful implementation.

2.0 MATHEMATICAL BASIS FOR SECTOR FOCUSING

We will describe a derivation of SF that is specifically designed to demonstrate (1) how the technique achieves stable MFP by restricting the processing to a reduced set of eigenvectors of the CSM and (2) how the set of eigenvectors used may be adjusted by varying the size, shape, and dimensionality of the sector aperture.

2.1 Rationale

The SF method is designed to eliminate sensitivity to mismatch that is accentuated by the presence of a large correlated noise component. The rationale behind SF is best understood in terms of the eigenvectors z_n and eigenvalues λ_n of the CSM (denoted here by K) and their contribution to the ML estimator. The matrix K consists of averaged cross-correlations between the complex acoustic pressures P_n measured on the N hydrophones of an array and may be written

$$K = <\mathbf{PP}^\dagger> . \tag{1}$$

$\mathbf{P}$ is a column vector whose entries are the P_n, $\dagger$ denotes conjugate transpose, and $<...>$ denotes an average over time samples (snapshots). The acoustic pressure field from which K is derived is due to a source at range r_0 and depth z_0 from the hydrophone array superimposed on the ambient noise field, which is due to surface waves, wind, shipping, and other sources. In the case considered here, more hydrophones than waveguide modes are used to construct the replica vectors $\mathbf{e}(r,z)$, whose entries are the predicted complex pressures at the hydrophone locations due to an assumed source at location (r,z). In this case there are eigenvectors of K (those with the smallest eigenvalues) that are orthogonal to all $\mathbf{e}(r,z)$. Since the eigenvectors contribute to the ML estimator through their inner products with the replica vectors according to

$$\text{ML } (r,z) = 1 / \mathbf{e}^\dagger(r,z) K^{-1} \mathbf{e}(r,z) = 1 / \sum_{n=1}^{N} \lambda_n^{-1} | z_n^\dagger \mathbf{e}(r,z) |^2 \tag{2}$$

(with $K z_n = \lambda_n z_n$), those eigenvectors that are orthogonal to the replicas make a null contribution. However, when (any kind of) mismatch is present this is no longer the case. These orthogonal inner products no longer vanish, and their unwanted contributions to the ML estimator are amplified because they are weighted by the reciprocals of the smallest eigenvalues of K. Their presence may seriously degrade the performance of the ML estimator. Sector focusing seeks to diminish this degradation by eliminating the destabilizing terms from the summation in Eq. (2). This is achieved by forming a projection matrix from the most significant eigenvectors (those with the largest eigenvalues) of a covariance matrix formed from the superposition of many independent simulated sources at variable locations within the sector into which the focusing is concentrated. Sector focusing allows the processing to occur only on the eigenvectors that the source would energize were the source in the sector being processed. This reduces the instability induced by mismatch errors while it improves the input signal-to-noise ratio.

Sector focusing cannot determine (a priori) which eigenvectors of K have a significant projection on the signal arrival, but it can and does determine which eigenvectors are needed to describe a source from a given physical sector. Simply put, SF asks the question, "If a source were in this sector, which eigenvectors of K would it project onto?" It then uses only the contributions from these predetermined eigenvectors in the formation of the estimator. In so doing, it trades some resolution for significant stability against mismatch errors.

2.2 Formal Derivation of the Estimator

We can construct the SF estimator to restrict the processing to only those eigenvectors of the CSM that could be involved in describing the source, if it were in the sector, in the following manner. Consider a linear filter $w^{\dagger}Kw$ and require the high-resolution weight vector w for this filter to have minimal projection outside of the subspace spanned by those eigenvectors. If we label the projection matrix described in the last section as V, then this "sector-focusing" constraint takes the form $w^{\dagger}w = w^{\dagger}VV^{\dagger}w$. The sector-focused ML estimator is obtained by optimizing the filter $w^{\dagger}Kw$ for minimum variance, subject to this sector-focusing constraint, together with the usual "distortionless-look" constraint $w^{\dagger}e = 1$. To determine w we must therefore minimize the dual constraint cost function

$$\Gamma = w^{\dagger}Kw + \lambda_1 Re(w^{\dagger}e - 1) + \lambda_2 w^{\dagger}(I - VV^{\dagger})w , \qquad (3)$$

where λ_1 and λ_2 are Lagrange undetermined multipliers and I is the identity matrix. The minimization is accomplished by setting the derivative of Γ with respect to $w^{\dagger}$ to zero, i.e.

$$\partial\Gamma/\partial w^{\dagger} = Kw + \lambda_1 e/2 + \lambda_2(I - VV^{\dagger})w = 0 . \qquad (4)$$

If we premultiply the RHS of Eq. (4) by $V^{\dagger}$ and replace w by Va (a is any $k \times 1$ complex vector and k is the rank of V), we obtain

$$V^{\dagger}KVa + \lambda_1 V^{\dagger}e/2 + \lambda_2(V^{\dagger} - V^{\dagger}VV^{\dagger})w = 0 . \qquad (5)$$

The columns of V are generally orthonormal vectors, so that $V^{\dagger}V = I$. Hence, the third term on the LHS of Eq. (5) vanishes and the expression reduces to

$$w + \lambda_1 V(V^{\dagger}KV)^{-1} V^{\dagger}e/2 = 0 . \qquad (6)$$

If we premultiply this equation by $e^{\dagger}$ and use the constraint $w^{\dagger}e = 1$, we obtain an expression which can be solved for λ_1, i.e.,

$$\lambda_1 = -2 / e^{\dagger}V(V^{\dagger}KV)^{-1} V^{\dagger}e . \qquad (7)$$

Substituting Eq. (7) back into Eq. (6) gives the weight vector

$$w = V(V^{\dagger}KV)^{-1} V^{\dagger}e / e^{\dagger}V(V^{\dagger}KV)^{-1} V^{\dagger}e , \qquad (8)$$

and further substitution of w into the filter $w^{\dagger}Kw$ gives the SF estimator

$$\text{SF} = \mathbf{w}^\dagger K \mathbf{w} = \frac{\mathbf{e}^\dagger V \left(V^\dagger K V \right)^{-1} V^\dagger}{\mathbf{e}^\dagger V \left(V^\dagger K V \right)^{-1} V^\dagger \mathbf{e}} K \frac{V \left(V^\dagger K V \right)^{-1} V^\dagger \mathbf{e}}{\mathbf{e}^\dagger V \left(V^\dagger K V \right)^{-1} V^\dagger \mathbf{e}}$$

$$= \frac{\mathbf{e}^\dagger V \left(V^\dagger K V \right)^{-1} V^\dagger K V \left(V^\dagger K V \right)^{-1} V^\dagger \mathbf{e}}{\left[\mathbf{e}^\dagger V \left(V^\dagger K V \right)^{-1} V^\dagger \mathbf{e} \right]^2}$$

$$= \frac{1}{\mathbf{e}^\dagger V \left(V^\dagger K V \right)^{-1} V^\dagger \mathbf{e}} . \tag{9}$$

Inspection of the last line of Eq. (9) shows that V pre- and post-multiplies K, and therefore projects the covariance matrix into the space of the columns of V. It similarly projects the replica vectors $\mathbf{e}$. By this means, processing is concentrated on those eigenvectors that describe sources within the sector to which V corresponds.

2.3 Sector Limits

From the previous discussion, the set of eigenvectors used in processing is clearly determined by V, which is in turn dependent upon the choice of sector parameters. To implement SF, the sector shape and size (i.e., the range extent and depth extent), as well as the processing dimensionality, must be decided. These parameters may be adjusted to achieve the desired estimator performance. The practical choice of values for a specific application is frequently difficult and requires some experience. However, a general guideline is that as sector size and dimensionality are increased, resolution is improved and stability is reduced. To illustrate this feature and to provide some intuitive feeling for the technique, we will examine the theoretical behavior of the SF estimator in two special cases.

2.3.1 The "Small" Sector Limit

If the sector size is made smaller, the processing becomes more stable and the resolution decreases. The *small sector limit* occurs when the sector shrinks to a single point. In this case, the sector has an essential dimensionality of one, i.e., it only takes one eigenvector to describe data from the sector. The V matrix is therefore an $N \times 1$ matrix (i.e., a vector, which has unit norm because $V^\dagger V = I$). In the implementation of SF used here, where the sector surrounds the search point (a very typical implementation), the V matrix then becomes the replica vector itself at the search point. Thus, $V \equiv \mathbf{e}$, where $\mathbf{e}^\dagger \mathbf{e} = 1$. If we now substitute $\mathbf{e}$ for V in the SF estimator Eq. (9) we find

$$\text{SF} = \frac{1}{\mathbf{e}^\dagger \mathbf{e} \left(\mathbf{e}^\dagger K \mathbf{e} \right)^{-1} \mathbf{e}^\dagger \mathbf{e}} = \frac{1}{\left(\mathbf{e}^\dagger K \mathbf{e} \right)^{-1}} = \mathbf{e}^\dagger K \mathbf{e} , \tag{10}$$

which is just the Bartlett estimator [4]. The small sector limit of SF processing is Bartlett processing, which indicates that SF can always be made to achieve the Bartlett conditions of maximum stability (and minimum resolution) by collapsing the sector until it becomes a single point at the search location.

2.3.2 The "Large" Sector Limit

As the sector size is increased, a stage is eventually reached where further increases in size have no effect on the processing. In this *large sector limit*, the sector encompasses such a large part of the search space that the columns of V, which describe sources placed throughout the sector, and therefore, in this case, throughout a large part of the waveguide, span the same vector space as the columns of the modal matrix U (the matrix whose elements are the sampled values of the depth modal functions at the array element depths) [7,10]. This may be formally expressed $V = UX$, where V and U are both $N \times M$ ($M < N$ is the number of modes), and X is $M \times M$. Since U and V span the same vector space, X has full rank, so its inverse is defined. If we now substitute UX for V in the SF estimator Eq. (9), we find

$$SF = \frac{1}{\mathbf{e}^\dagger UX \left(X^\dagger U^\dagger KUX \right)^{-1} X^\dagger U^\dagger \mathbf{e}} = \frac{1}{\mathbf{e}^\dagger UXX^{-1} \left(U^\dagger KU \right)^{-1} X^{\dagger-1} X^\dagger U^\dagger \mathbf{e}}$$

$$= \frac{1}{\mathbf{e}^\dagger U \left(U^\dagger KU \right)^{-1} U^\dagger \mathbf{e}}, \tag{11}$$

which is just the RML estimator [34]. The large sector limit of SF processing is RML processing. As we will see, this limit may generally be achieved using sector dimensions significantly smaller than those of the waveguide.

RML usually gives higher resolution, with lower stability, than the Bartlett processor. However, as we shall show, the application of SF with a careful choice of sector dimensions lying between the small and large limits will generally perform better (i.e., give higher resolution while maintaining stability) than both of these other two methods.

3.0 THE SIMULATED EXPERIMENT

To illustrate the effects of different implementations of SF, we performed a series of simulations in a representative shallow-water environment. In this section we describe the propagation model used to perform the required acoustical calculations, the experimental geometry and environmental parameters, the method by which mismatch variations were introduced, and the quantification of the ambiguity surfaces.

3.1 The SUPERSNAP Propagation Model

The acoustic calculations for this report were performed using the SACLANTCEN Normal-Mode Acoustic Propagation (SNAP) model [38]. The model divides the environment into three layers, as shown in Fig. 1. The water column, which incorporates a depth-variable sound speed with constant density and volume attenuation, is underlain by a layer of sediment, which also allows a depth-variable sound speed with constant density and attenuation. The subbottom is a semi-infinite half-space with depth-independent sound speed, density, and attenuation. For the depths and frequencies considered here, the model predicts 20 propagating modes. Of these, only the lowest 10 were used for the field calculations, since the remaining modes were trapped in the sediment layer and, therefore, highly attenuated.
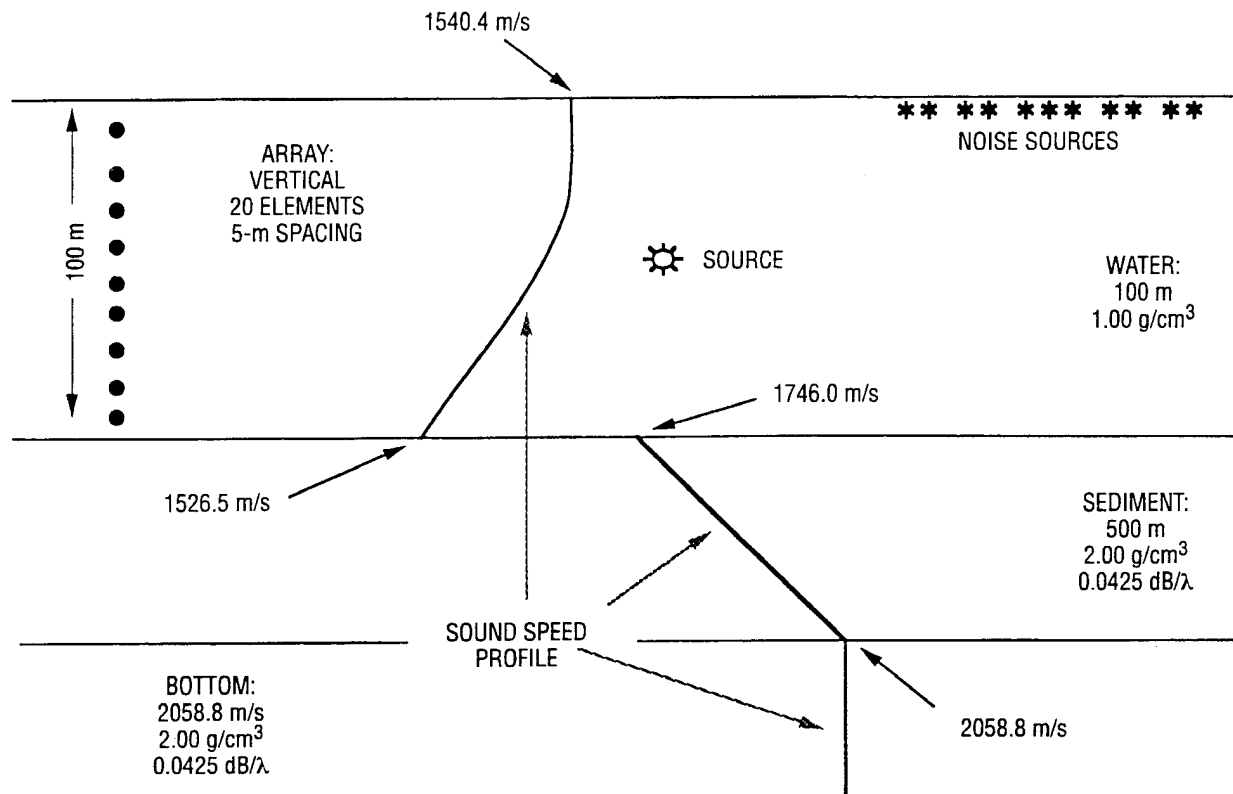
Fig. 1 — Waveguide environment and geometry; environmental parameters are indicated, including the sound speed profile in the water, sediment, and bottom layers. The experimental arrangement of source and receiving array are shown, as is the random placement of noise sources used to determine the correlated noise component in the covariance matrix.

3.2 Configuration of the Experiment

The environment in which the experiment simulated here was performed consists of a range-independent, shallow-water waveguide of 100-m depth and 1 g/cm^3 density overlaying a sediment layer of 500-m thickness, 2 g/cm^3 density, and an acoustic attenuation of 0.0425 dB/λ at the 150-Hz source frequency. The water and sediment layers are underlain by an isospeed, semi-infinite basement. The sediment has a constant compressional velocity gradient: the sound speed increases linearly from 1746.0 m/s at the water-sediment interface to 2058.8 m/s at the sediment-basement interface. The basement has a specific density of 2 g/cm^3 and a constant compressional velocity of 2058.8 m/s. Since the basement has properties matching the base of the sediment layer, reflections at the sediment-basement interface may be neglected. Shear wave propagation was not incorporated into the problem. These parameters are typical of a continental shelf environment, such as the environment off the coast of Panama City, Florida.

A vertical array of 20 evenly spaced hydrophones spanning the water column is suspended in the waveguide and extends from 3 to 98 m in depth. The hydrophones, therefore, have a spacing of 5 m, which is the half-wavelength value at 150 Hz. The 150-Hz narrow-band source was placed 5 km from the array at depths of 15, 50, and 75 m. The search region to locate the source extends from 0 to 100 m in depth and from 3000 to 7000 m in range. The grid spacing is 50 m in range and 1 m in depth.
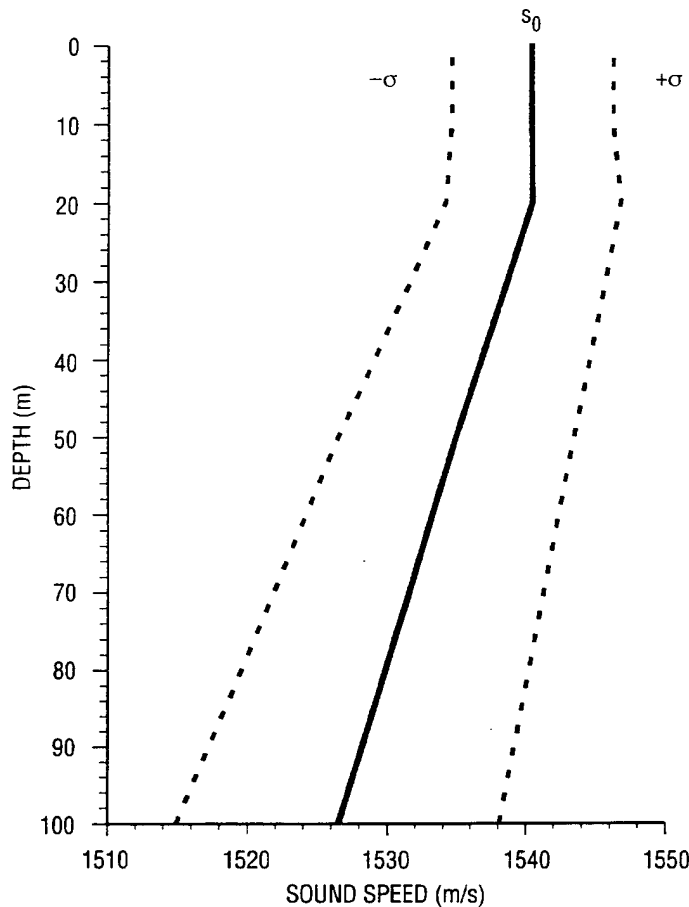
Fig. 2 — Mean and mismatched sound speed profiles. Solid line indicates the mean summer sound speed profile used to calculate the replica field; dotted lines represent profiles that deviate from the mean by $\pm\sigma$, where σ is the statistical standard deviation. Since both s_0 and σ are functions of depth, by adding percentages of the standard deviation at each depth, perturbations of the mean profile change both the profile gradient and the offset.

Shipping noise was modeled by simulating the random movement of 40 distant sources whose ranges were constrained to lie in a random pattern within 10 to 100 km of the receiving array. These sources were placed at a 7-m depth and were allowed to move at a constant speed of 12 kt between simulated snapshots taken at an interval of 1 s. Levels for the source and modal noise were both 30 dB, giving 0 dB signal-to-(modal)-noise ratio. White noise at a level of 10 dB was also added.

3.3 Water Sound Speed Profile Variations

The focus of our investigations was the performance of the SF estimator in the presence of a water sound speed profile mismatch. Figure 2 shows a typical summer sound speed profile (the central solid line) for a midlatitude shallow-water environment, which was derived from database sources [39]. It is seen to be strongly downward refracting. A pair of dotted lines can be seen to the left and right of this profile. These lines represent sound speed profiles that deviate from the central profile by $\pm1\sigma$, as determined statistically from the database. Careful examination of Fig. 2 shows that the $\pm1\sigma$ deviation of the sound speed profile is neither uniform nor symmetrical and gradually increases with depth. The effects of mismatch of the water sound speed profile were investigated by first using the central profile to calculate the replica acoustic pressure field, against which the detected field was to be matched for a grid of estimated source depths and ranges. Mismatches were then introduced by varying the sound speed profile used to simulate the detected pressure field by selected amounts within the $\pm1\sigma$ envelopes. The mismatches were accomplished in the following manner. Let $s_0(z)$ be the mean sound speed profile and $\sigma(z)$ be the standard deviation about this mean profile at each water depth z. If the sound speed is perturbed by a percentage α of the standard deviation at each depth, the mismatched profile is given by

$$c_\alpha(z) = s_0(z) \pm \frac{\alpha\sigma(z)}{100} . \tag{12}$$

Since $\sigma(z)$ is depth dependent, the use of Eq. (12) ensures that the profile gradient is varied, together with the offset, so that mismatch is simulated which is realistic from the point of view of matched-field processing. In this study, values of α were used which corresponded to -40% and

–50% deviations from the mean profile. The –50% value represents a large mismatch. Beyond this value no meaningful assessment of the performance of the SF estimator could be made, since even the Bartlett estimator, which is considered normative, then failed. Here, we investigated adjustments in performance of the SF estimator as sector size, shape, and dimensionality were varied under conditions of severe sound speed profile mismatch of this type.

3.4 Statistical Quantification of the Ambiguity Surfaces

To provide a means of quantifying the ambiguity surfaces produced by the SF estimator under the various implementations, and a measure of peak discrimination, the peak value (P), mean background level (μ), and standard deviation of the background (σ) were calculated over the search region for the surface. The mean level was calculated by excluding a 13-point by 13-point box (600-m range by 12-m depth) surrounding the peak location. The measurements of peak-to-background ratio (PBR) used were then given by

$$PBR = 10 \ \log[(P-\mu)/\sigma] \ . \tag{13}$$

This measure can be thought of as giving the height of the peak above the background in units of the standard deviation and is expressed in decibels.

4.0 SIMULATIONS

4.1 Forming a Sector

For this study we used the "sliding" sector implementation of SF described in previous work [36]. In this method, a fixed-shape (in our case rectangular) sector is moved along with the search point, which is contained within it (see Fig. 3). We then calculated the replica vectors for a cartesian grid (5 rows and 5 columns) of sample points within the sector. The spacing of the rows and columns is determined by the overall range and depth extents of the sector. The sector covariance matrix, Q, was formed by averaging the outer products of the replica vectors from the points in the sector, i.e., $Q = \langle e(r_\sigma, z_\sigma) \ e(r_\sigma, z_\sigma)^\dagger \rangle$. The average was formed by a superposition of independent sources at the locations (r_σ, z_σ) within the sector. The number of points in the sector (i.e., 25) was kept constant throughout the study. This number always exceeded the number of modes supported by the
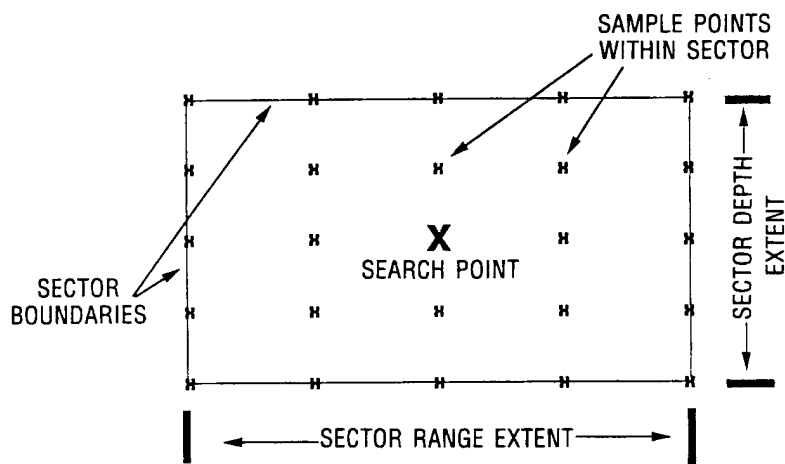

Fig. 3 — Schematic layout of search sector. Once the range and depth extents have been chosen, the sector space is spanned by a 5×5 grid of sample points. The sector covariance matrix is formed by averaging the outer products of the replica vectors for these points. In the example shown here, the central sample point is also the search point.

waveguide (i.e., 10) and also ensured that Q, from which the projection matrix V was derived, had full rank.

4.2 Essential Dimensionality

Although the sector covariance matrix Q is formed from sufficient independent replicas from within the sector to have full rank, its "essential" or effective rank (or dimensionality) may be much smaller. If the sector is very small, it may only require (say) one or two replicas to accurately describe sources from within it. The essential dimensionality of its corresponding covariance matrix will then be correspondingly either one or two. As the sector is made larger, the sources spaced within it more thoroughly represent the modal structure of the waveguide, and the rank of Q increases. If we perform an eigenvector decomposition of Q we may, for the purposes of this study, define its essential dimensionality (k) as the number of eigenvalues greater than 1% of the largest eigenvalue. (Recall that V is formed by using the eigenvectors belonging to the largest k eigenvalues of Q as its columns.) In Fig. 4(a), we show the eigenspectrum of Q for a 5-m × 1-m sector. This small sector has $k = 1$ (the eigenvalues for $n > 1$ are seen to be zero). In contrast, the 700-m × 40-m sector, whose eigenspectrum is shown in Fig. 4(b), has $k = 10$. We will see that, as the size of the sector increases, the value of k also increases until it reaches the limit of the number of modes.

To see how the essential dimensionality changes with sector range and depth extent, we plot the maps of k shown in Fig. 5 (a–c). These maps were constructed by varying the size and shape of a sector surrounding a search point placed at 15-, 50-, and 75-m depths, respectively. The x axis in each case shows the range extent of the sector, while the y axis shows the depth extent. The contour lines mark the borders between dimensionality regions. We see that, as expected, the smallest sectors have a dimensionality of one. The largest ones have a dimensionality of 10 (the number of modes). The dimensionality does not increase beyond this value, however large the sector becomes. We note from these figures that we can attain the same k using differently shaped (e.g., tall-thin or short-wide) sectors. It is also evident, by comparing Fig. 5 (a–c), that the value of k for a particularly shaped sector may also vary with sector depth.

4.3 Demonstration of the Small Sector Limit

In Sec. 1 (Eq. (10)), we showed formally that SF is identical to the Bartlett estimator when the V matrix is replaced by the replica at the search point. We can demonstrate that the Bartlett estimator is equivalent to the small sector limit by performing a simulation in which the range and
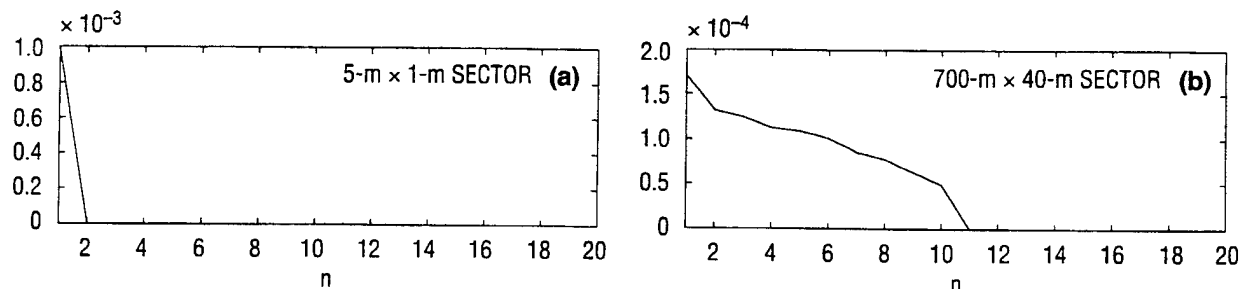

Fig. 4 — Eigenspectra of small and large sectors. Eigenvalues of the sector covariance matrix are plotted as a function of the eigenvector number, beginning with $n = 1$. Both sectors are centered over a search point placed at 50-m depth.
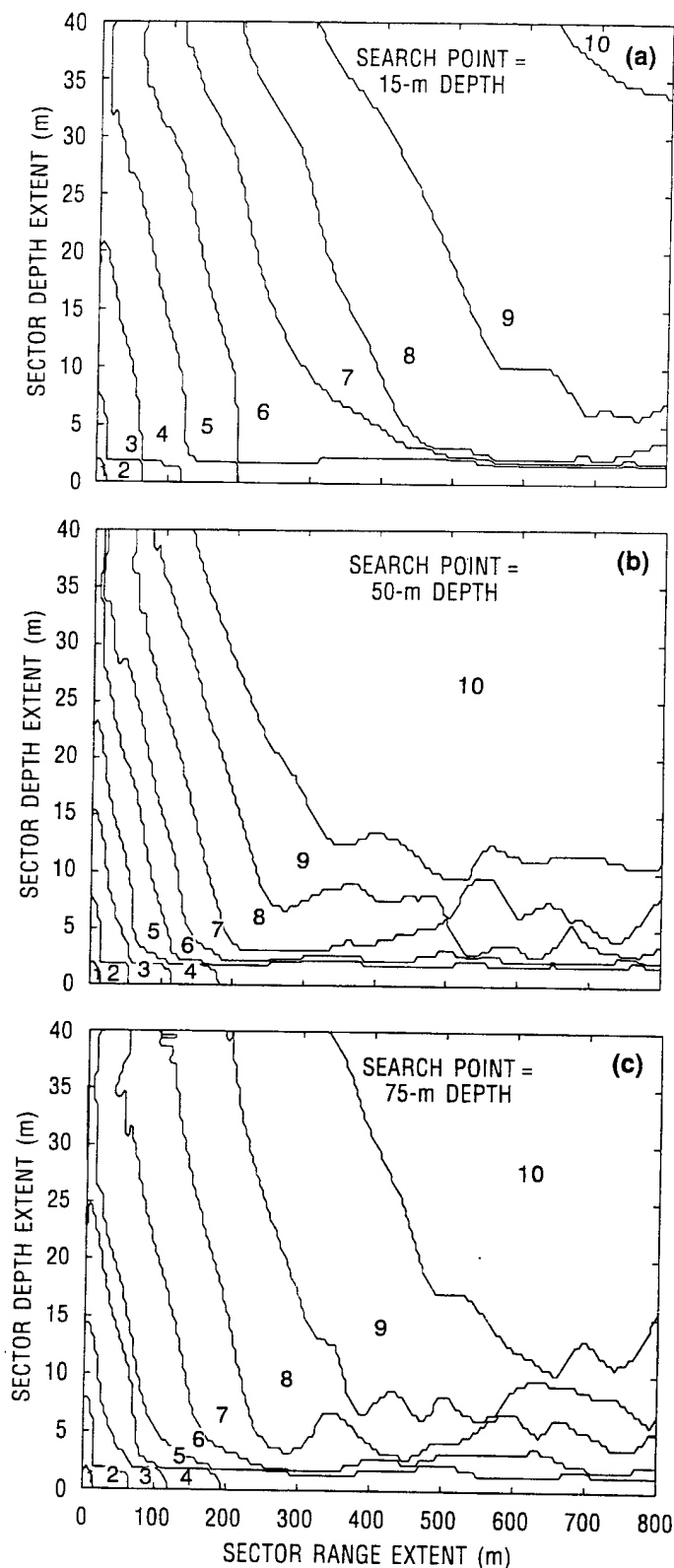
Fig. 5 — Sector dimensionality maps. Contours separate regions of different essential dimensionality as the sector range and depth extents are increased. The 1% criterion has been used. The essential dimensionality varies with the sector size and shape, and also the depth of the search point over which the sector is centered.

depth extents of the sector are reduced to such a degree that all of the replica vectors within the sector become effectively identical to each other and to the search point replica itself. In such a case, the sector covariance matrix, Q, would approach singularity, with a rank of one, and the eigenvector corresponding to the one non-zero eigenvalue would be equal to the replica at the search point.

In Fig. 6(a) we show a Bartlett ambiguity surface for a source placed at a range of 5000 m and at 75-m depth in the waveguide, for a case in which the water sound speed profile is mismatched by −50% from the mean profile, as prescribed by Eq. (12). The Bartlett estimator correctly locates the source, but the ambiguity surface is characteristically difficult to interpret with high background sidelobes and a broad signal peak. The value of PBR is 8.19 dB. We will now perform SF, using a sector size of 5 m × 1 m. Inspection of Fig. 5(c) shows that, with this sector size, the essential dimensionality of Q is 1. If we use only the one "large eigenvector" of Q to form the V matrix (which is still $\approx$ e), and apply the estimator in Eq. (9) in an equivalent manner to Eq. (10), we obtain the surface shown in Fig. 6(b). This surface is practically identical to the Bartlett surface, with a PBR of 8.18 dB. We see that SF has the same ability to discriminate the source peak as Bartlett (but also achieves the same robustness) in the small sector limit.

Sector focusing can also be "forced" to give the same performance as Bartlett when the sector size is increased such that the essential dimensionality is actually greater than 1. In Fig. 7 we see SF for the same mismatch case as Fig. 6, but using a sector size of 5 m × 5 m. Fig. 5(c) shows that the essential dimensionality for this case is 2. One of the two eigenvalues is much larger than the other and dominates Q. Since the sector is still quite small, the eigenvector corresponding to this eigenvalue remains strongly representative of
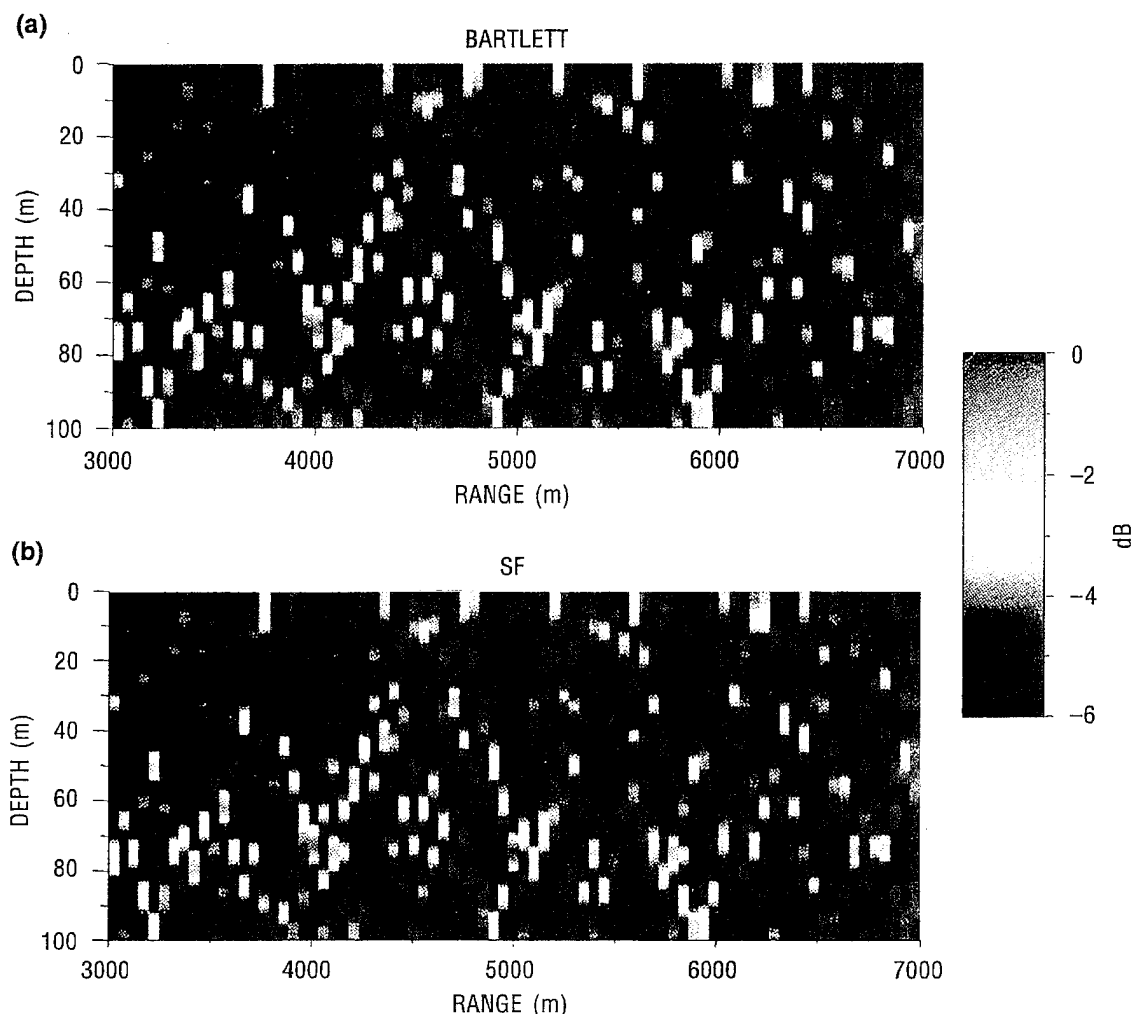
(a)

BARTLETT

(b)

SF

Fig. 6 — Comparison of Bartlett and SF in the "small" sector limit. Ambiguity surfaces are calculated for a source placed at 5000-m range and 75-m depth in the waveguide, with –50% mismatch of the sound speed profile. A 5-m × 1-m sector was used for the SF case. The surfaces are practically identical. (a) PBR = 8.19 dB and (b) PBR = 8.18 dB.

the search point replica within the sector (i.e., it is still ≈ **e**). If we use just this one large eigen-vector to form the V matrix and apply the estimator as indicated by Eq. (10), we obtain the ambiguity surface shown in Fig. 7(a). Comparison with Fig. 6(a) shows that this is again very similar to the Bartlett surface, with a PBR of 8.08 dB.

With the 5-m × 5-m sector, the additional dimensionality (i.e., the second available eigenvec-tor) can be used to improve the quality of the ambiguity surface and to reduce the background sidelobe levels without losing processor stability. Figure 7(b) shows the ambiguity surface pro-duced by SF when V contains both the eigenvector used to give Fig. 7(a) previously and the eigenvector corresponding to the second smaller, but still significant, eigenvalue. In Fig. 7(b), we see the source correctly predicted at the input location, but now the sidelobe background level has been reduced to give a PBR of 9.33 dB.

What is the result of increasing sector size yet further? Figure 8 is produced with a sector size of 35 m × 5 m. Figure 5(c) indicates that the corresponding Q has an essential dimensionality of 3.
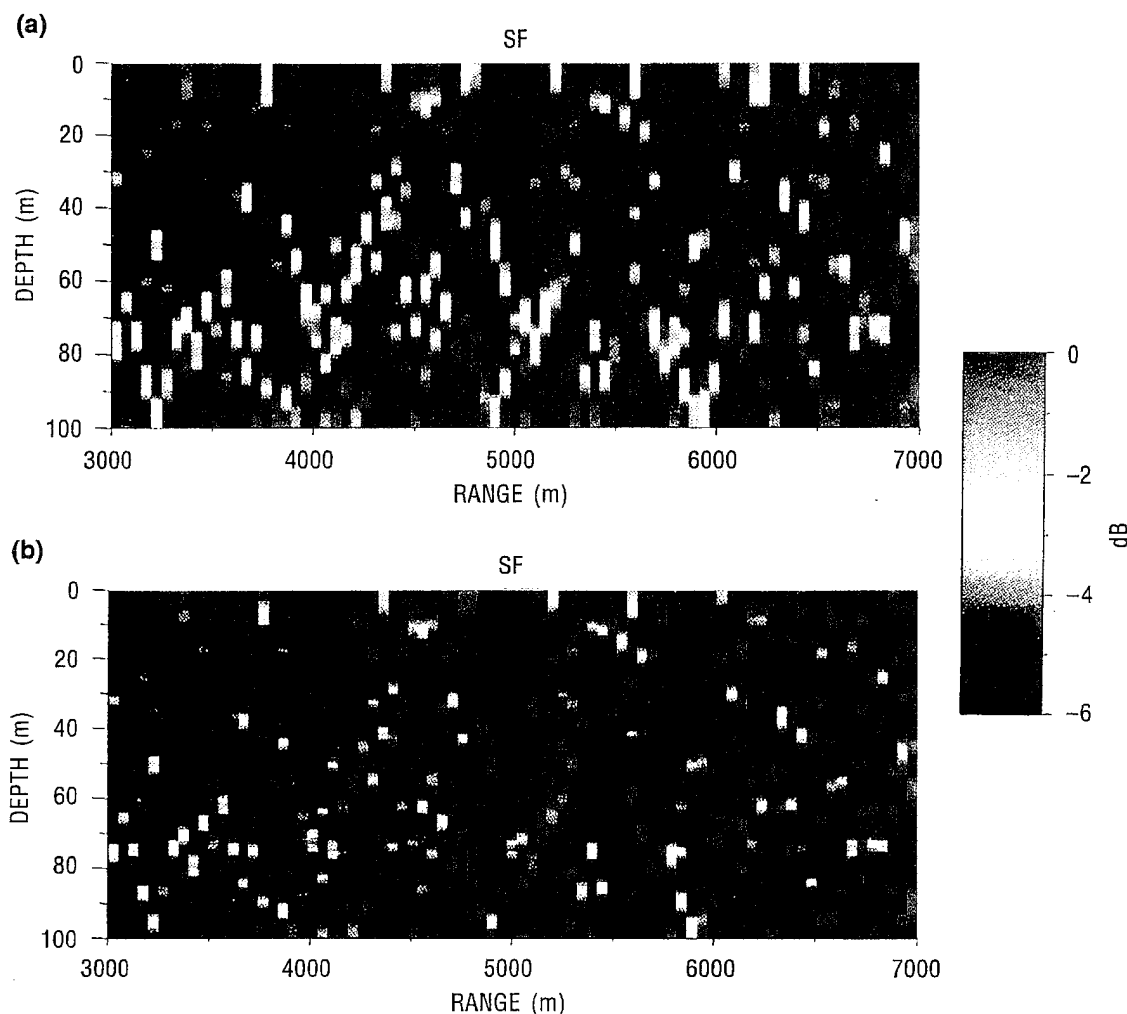
Fig. 7 — "Forced" Bartlett behavior using SF with sector larger than the "small" sector limit. Both of the SF surfaces are calculated for a source placed at 5000-m range and 75-m depth in the waveguide, with –50% mismatch of the sound speed profile. A sector 5-m × 5-m is used, which has an essential dimensionality of 2. (a) Only the largest eigenvector is used. The surface is very similar to Fig. 6(a), PBR = 8.08 dB and (b) both available significant eigenvectors are used, PBR = 9.33 dB.

If we use just the two largest eigenvectors of Q to form V and apply SF, we get the surface shown in Fig. 8(a). This surface has a PBR of 9.27 dB and is quite similar to Fig. 7(b). However, if we increase V to include all three of the significant eigenvectors of Q, thus using all of the available dimensionality of the sector, we obtain Fig. 8(b). In this case, SF fails to correctly identify the source, since it puts its largest peak at a range of 4000 m. The sidelobe level has also increased, reducing the PBR to 8.89 dB. This result may be interpreted by appealing to Eq. (2). It appears that a mismatch of the sound speed profile by –50% is significantly large when the source is placed at 75-m depth. Most of the terms in the summation in Eq. (2) are destabilized by this degree of mismatch; and SF must be implemented in such a way that processing can be allowed on only the two largest eigenvectors, if stable estimation is to be achieved. The two eigenvectors may be selected by using a 5-m × 5-m sector, and using all of the available dimensionality; or by using a 35-m × 5-m sector (or other comparable sector choice), and using only the two largest eigenvectors.
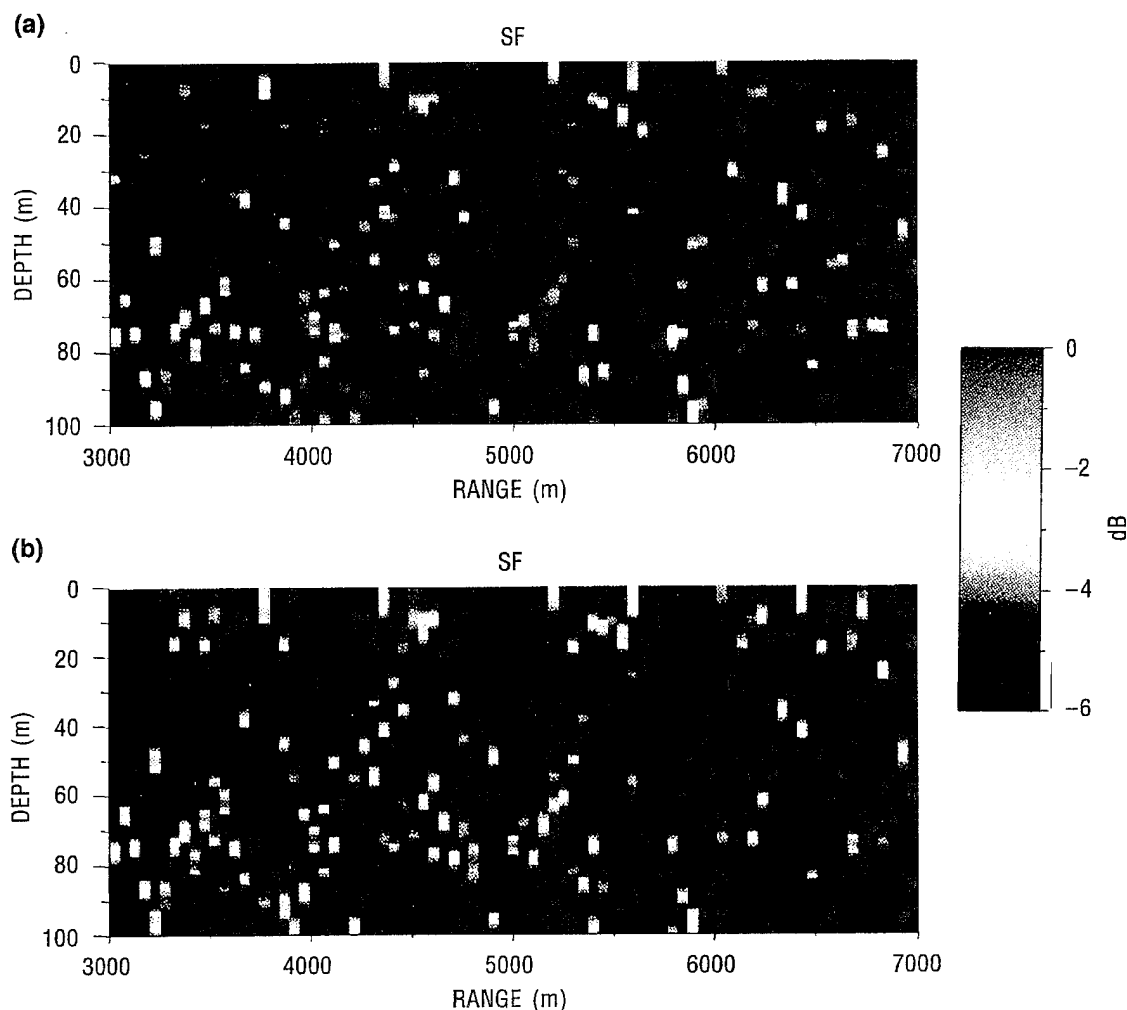
Fig. 8 — SF with increased sector size. Both surfaces are calculated for a source placed at 5000-m range and 75-m depth in the waveguide, with −50% mismatch of the sound speed profile. A sector 35-m × 5-m is used, which has an essential dimensionality of 3. (a) The two largest eigenvectors are used, the source is correctly located, PBR = 9.27 dB and (b) all three available significant eigenvectors are used. SF fails as it incorrectly locates the source at 4000-m range and 73-m depth, PBR = 8.89 dB.

4.4 Demonstration of the Large Sector Limit

If the amount of mismatch is less than that experienced in the case previously described, it may be possible to use a larger sector with higher essential dimensionality to significantly reduce the sidelobe background level while maintaining estimator stability. Returning to Eq. (2): this means that fewer of the terms in the summation will be destabilized by the mismatch, and that the sectors may be designed to select more eigenvectors for processing. As the number of terms increases, then SF looks more like ML, which performs very well (returning very accurate source location predictions with good sidelobe reduction) under conditions of low mismatch.

In a waveguide, the maximum dimensionality that can be achieved is equivalent to the number of modes M, regardless of how large the sector is made. In Fig. 9, we look at the case of a source placed at a 5000-m range and 15-m depth in the waveguide, with the sound speed profile mismatched by −40%, representing a significantly less mismatched case than the 75-m, −50% example used
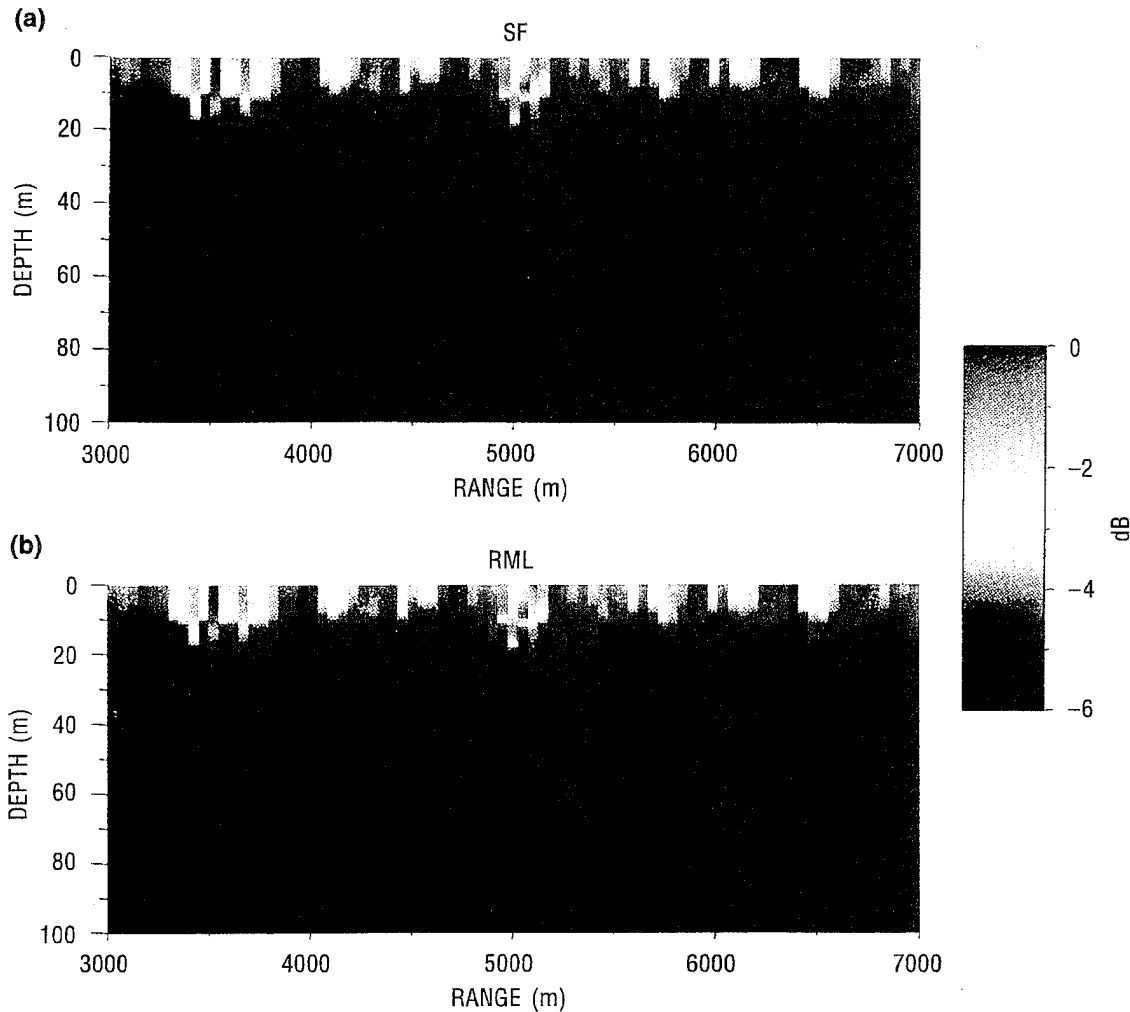
Fig. 9 — Comparison of SF in the "large" sector limit and RML. Ambiguity surfaces are calculated for a source placed at 5000-m range and 15-m depth in the waveguide, with –40% mismatch of the sound speed profile. A 700-m × 40-m sector was used for the SF case. The surfaces are indistinguishable. (a) SF, PBR = 9.27 dB and (b) RML, PBR = 9.27 dB.

earlier. Figure 9(a) shows the result of implementing SF with a 700-m × 40-m sector. Inspection of Fig. 5(a) shows that the Q for a sector of this size has an essential dimensionality of 10, which is the value of M. According to the argument in Sec. 2.3, this should place SF well into the large sector limit and produce identical results to RML. Figure 9(b) shows the RML surface for the same case. Close comparison reveals that it is, indeed, identical to Fig. 9(a). Both methods give the same PBR of 9.27 dB.

Although, as we have seen, it is possible to implement SF for the above case using a sector dimensionality of 10, this is not necessarily the most effective implementation. We may, and in most cases will, achieve best results using a sector size that is intermediate between the small and large sector limits. In Fig. 10 we plot (for the same 15 m, −40% mismatch case depicted in Fig. 9) the variation of PBR for a series of implementations of SF, with sector sizes increasing to raise the essential dimensionality incrementally from 1 to 10. After some initial oscillation, the value of PBR improves steadily, reaching a peak of 11.86 dB with a sector size of 400 m × 20 m, which has an essential dimensionality of 9. When the sector size is further increased to 700 m × 40 m to give

an essential dimensionality of 10, which is the case shown in Fig. 9(a), the PBR falls to 9.27 dB. The "best" performance is achieved with an essential dimensionality of 9 in this case. In the 75-m, −50% case depicted in Figs. 7 and 8, it was achieved with an essential dimensionality of 2. The most effective way of implementing SF will clearly vary according to individual cases, and must be determined empirically. However, by using a small sector the processor can always be made as stable as Bartlett, and by using a large sector it can be made to perform identically to RML. Generally, the sector size can be adjusted to give better results than either of these two other methods. For the 75-m source with −50% mismatch, a 5-m × 5-m sector with essential dimensionality 2 gives the optimum result, which is intermediate between Bartlett and RML, but closer to the small sector (Bartlett) limit. In contrast, for the 15-m source with −40% mismatch, a 400-m × 20-m sector with essential dimensionality 9 gives the optimum result, which is also intermediate between Bartlett and RML but, in this case, closer to the large sector (RML) limit.

Just as SF can be forced into giving Bartlett behavior by selecting the one largest eigenvector of Q when the sector is actually larger than the small sector limit, so it may be similarly forced into giving RML behavior by using the 10 largest eigenvectors of Q when the sector is smaller than the large sector limit. In Fig. 11, we plot (again for the same 15-m, −40% mismatch case used above) the variation of PBR for a series of implementations of SF, with sector sizes increasing in the same sequence used for Fig. 10. This time, however, the 10 largest eigenvectors of Q are used in every case, regardless of the essential dimensionality for any particular sector. We see that PBR falls from an initial value of 11.40 dB, with a 5-m × 1-m sector, to 9.18 dB for a 35-m × 5-m sector. It then
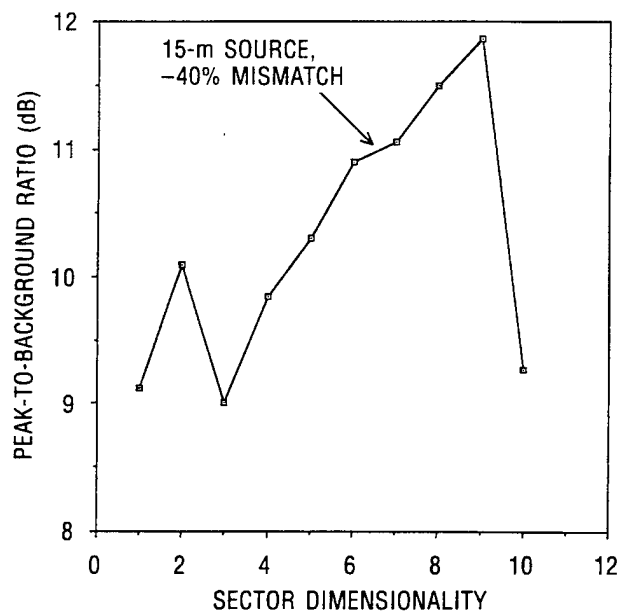

Fig. 10 — Variation of PBR with increasing sector dimensionality. Values are calculated for a source placed at 5000-m range and 15-m depth in the waveguide. A series of implementations of SF were performed with sector sizes increasing so that the essential dimensionality was raised incrementally from 1 to 10. The best performance (PBR = 11.86 dB) was obtained with a sector 400-m × 20-m, which has an essential dimensionality of 9.
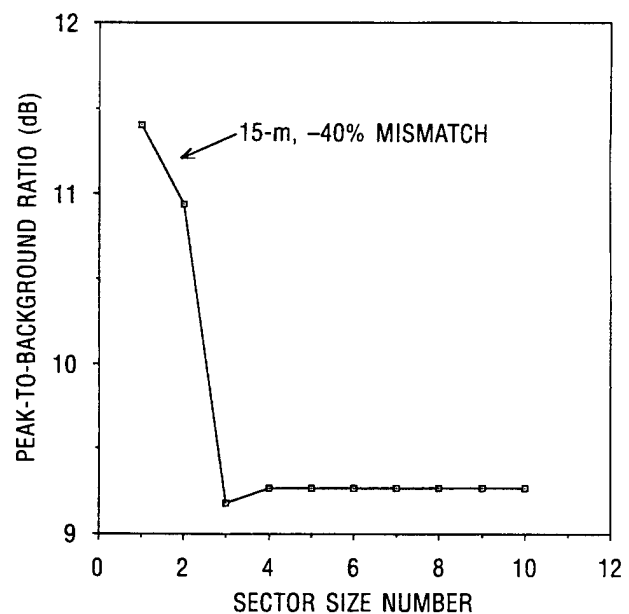
Fig. 11 — Variation of PBR with increasing sector size and constant dimensionality. Curves are calculated for a source placed at 5000-m range and 15-m depth in the waveguide. A series of implementations of SF were performed with sector sizes increasing in the same sequence used for Fig. 10, except the dimensionality was maintained at 10 throughout. The processor is "forced" to behave like RML when the sector is only 80-m × 10-m (sector size number 4), giving a PBR of 9.27 dB, which is equal to the RML value in Fig. 9(b). It maintains this performance as the sector size is increased to the "large" sector limit.

rises slightly to 9.27 dB and remains at this value, which is the RML value obtained in Fig. 9(b), as the sector size is further increased towards the large sector limit. Figure 11 shows that SF begins to reproduce RML behavior when the sector size is such that its essential dimensionality is only 4. What is the explanation? Possibly the 1% criterion we have set for counting large eigenvalues is too high. If it were lowered, then the essential dimensionality would reach higher values with smaller sector sizes, which may mean that the large sector limit (and RML behavior) is reached with much smaller sectors than the maps in Fig. 5 (which used the 1% criterion) indicate.

4.5 Variation with Mismatch

As mentioned, SF implementations must be optimized for the mismatch conditions encountered. To emphasize this feature of the processor, we will examine the effects of variable mismatch on two cases. In Fig. 12(a), we plot PBR against mismatch for a source placed at 50-m depth in the waveguide. The mismatch varies from −50% to +50% deviation from the mean profile, as prescribed by Eq. (12). Curves are plotted for SF (using a 150-m × 5-m sector with essential dimensionality 7) and Bartlett. We see that SF consistently outperforms Bartlett. When the mismatch is either zero or small, SF has a PBR 4–5 dB better than Bartlett, with stable and accurate location of the source. As the mismatch increases toward ±50% deviation, the improvement offered by SF falls to 1–2 dB, but it still returns accurate location estimates. In Fig. 12(b), we plot PBR against mismatch for a source placed at 75-m depth in the waveguide. The uppermost curve is the variation of PBR using SF with the 150-m × 5-m sector, as used in Fig. 12(a). When the mismatch is small it gives 5–6 dB improvement over Bartlett, but when the mismatch increases beyond ±10% deviation, SF becomes unstable and fails to correctly locate the source. This failure, indicated by the two vertical lines in the figure, is not surprising. The 150-m × 5-m sector has an essential dimensionality of 6
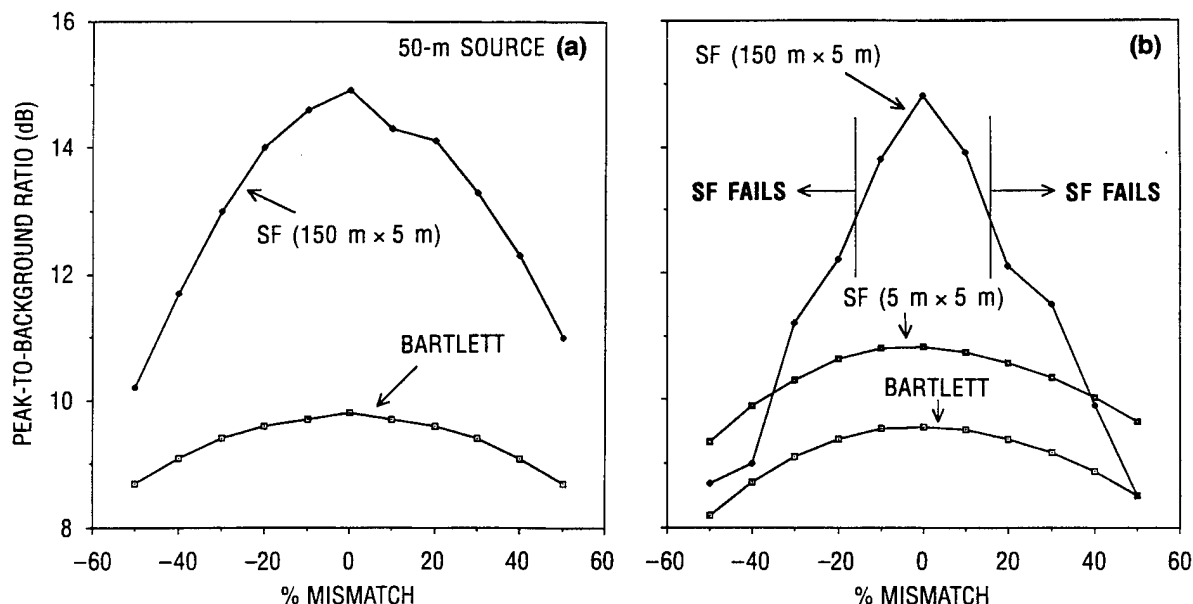

Fig. 12 — Variation of PBR with mismatch. PBR is plotted against percentage mismatch of the sound speed profile, as prescribed by Eq. 12. (a) Source is placed at 5000-m range, 50-m depth; SF is used with a 150-m × 5-m sector implementation and gives a better performance than Bartlett, while maintaining stability over the whole range of mismatch values. (b) Source is placed at 5000-m range, 75-m depth, and the 150-m × 5-m sector implementation of SF fails when the mismatch is greater than ±10%. The smaller sector implementation (5 m × 5 m) gives less improvement over Bartlett, but maintains stability.

for a 75-m source and we should expect, following our discussion of Figs. 7 and 8, that a sector with essential dimensionality of more than 2 would fail in this case. In Fig. 12(b), we also plot the variation of PBR for SF with a 5-m × 5-m sector, which has an essential dimensionality of 2. Here we find stable localization and a steady improvement of about 1.5 dB over Bartlett throughout the range of mismatch values. As a general rule, large sectors, leading to significant reductions in sidelobe levels, may be used if the mismatch is small. As the mismatch increases, the sector size must be reduced to maintain stability. If it is necessary to reduce the sector size to the small sector limit, SF will return the Bartlett result.

5.0 CONCLUSIONS

Sector focusing is a flexible matched-field signal processing technique that can be readily adapted to improve performance and maintain stability for different environmental and mismatch conditions. Sector focusing performance may be fine-tuned by changing the sector dimensionality (by adjusting sector size and shape) and by varying the number of eigenvectors in the projection matrix. In the small sector limit, SF performs identically to the Bartlett processor. In the large sector limit, it performs identically to the RML processor. It is generally possible, by making careful sector choices, to obtain stable processor performance that is significantly better than either of these other two methods.

6.0 ACKNOWLEDGMENTS

7.0 REFERENCES

[1] H. P. Bucker, "Use of Calculated Sound Fields and Matched-Field Detection to Locate Sound Sources in Shallow Water," *J. Acoust. Soc. Am.* **59**, 368–373 (1976).

[2] M. J. Hinich, "Maximum-Likelihood Signal Processing for a Vertical Array," *J. Acoust. Soc. Am.* **54**, 499–503 (1973).

[3] R. Klemm, "Range and Depth Estimation by Line Arrays in Shallow Water," *Signal Process.* **3**, 333–344 (1981).

[4] R. M. Heitmeyer, W. B. Moseley, and R. G. Fizell, "Full-Field Ambiguity Processing in a Complex Shallow-Water Environment," in *High Resolution Spatial Processing in Underwater Acoustics*, R. A. Wagstaff and A. B. Baggeroer, ed. (NORDA Book Contribution, NRL Publication, Stennis Space Center, MS, 1985) pp. 171–192.

[5] A. V. Oppenheim and R. W. Schafer, *Digital Signal Processing* (Prentice-Hall, New York, NY, 1971), pp. 548–549.

[6] C. T. Tindle, K. M. Guthrie, G. E. J. Bold, M. D. Johns, D. Jones, K. O. Dixon, and T. G. Birdsall, "Measurements of the Frequency Dependence of Normal Modes," *J. Acoust. Soc. Am.* **64**, 1178–1185 (1978).

[7] E. C. Shang, "Source Depth Estimation in Waveguides," *J. Acoust. Soc. Am.* **77**, 1413–1418 (1985).

[8] E. C. Shang, C. S. Clay, and Y. Y. Wang, "Passive Harmonic Source Ranging in Waveguides by Using Mode Filter," *J. Acoust. Soc. Am.* **78**, 172–175 (1985).

[9] E. C. Shang, "An Efficient High-Resolution Method of Source Localization Processing in Mode Space," *J. Acoust. Soc. Am.* **86**, 1960–1964 (1989).

[10] T. C. Yang, "A Method of Range and Depth Estimation by Modal Decomposition," *J. Acoust. Soc. Am.* **82**, 1736–1745 (1987).

[11] T. C. Yang, "Modal Beamforming Array Gain," *J. Acoust. Soc. Am.* **85**, 146–151 (1989).

[12] T. C. Yang, "Modal Shading Coefficients for High-Resolution Source Depth Localization," *J. Acoust. Soc. Am.* **87**, 668–672 (1987).

[13] T. C. Yang, "Effectiveness of Mode Filtering: A Comparison of Matched-Field and Matched-Mode Processing," *J. Acoust. Soc. Am.* **87**, 2072–2084 (1990).

[14] G. R. Wilson, R. A. Koch, and P. J. Vidmar, "Matched Mode Localization," *J. Acoust. Soc. Am.* **84**, 310–320 (1988).

[15] J. Capon, "High-Resolution Frequency-Wavenumber Spectral Analysis," Proceedings of IEEE, 1969, vol. 57, pp. 1408–1418.

[16] R. T. Lacoss, "Data Adaptive Spectral Analysis Methods," *Geophysics* **36**, 661–675 (1971).

[17] N. Owsley, "SONAR Array Processing," in *Array Signal Processing,* S. Haykin, ed. (Prentice-Hall, 1985).

[18] C. Feuillade, W. A. Kinney, and D. R. DelBalzo, "Shallow-Water Matched-Field Localization off Panama City, Florida," *J. Acoust. Soc. Am.* **88**, 423–433 (1990).

[19] J. Q. D Tran and W. S. Hodgkiss, "Matched-Field Processing of 200 Hz Continuous Wave (cw) Signals," *J. Acoust. Soc. Am.* **89**, 745–755 (1991).

[20] M. B. Porter, R. L. Dicus, and R. G. Fizell, "Simulations of Matched-Field Processing in a Deep-Water, Pacific Environment," *IEEE J. Ocean. Eng.* **OE-12**, 173–181 (1987).

[21] R. G. Fizell and M. B. Porter, "Bottom Effects on Matched-Field Localization Performance in the North Pacific," *J. Acoust. Soc. Am.* **81**(S1), S84 (1987).

[22] D. F. Gingras, "Methods for Predicting the Sensitivity of Matched-Field Processors to Mismatch," *J. Acoust. Soc. Am.* **86**, 1940–1949 (1989).

[23] R. M. Hamson and R. M. Heitmeyer, "Environmental and System Effects on Source Localization in Shallow Water by the Matched-Field Processing of a Vertical Array," *J. Acoust. Soc. Am.* **86**, 1950–1959 (1989).

[24] E. C. Shang and Y. Y. Wang, "Environmental Mismatching Effects on Source Localization Processing in Mode Space," *J. Acoust. Soc. Am.* **89**, 2285–2290 (1991).

[25] D. R. DelBalzo, C. Feuillade, and M. M. Rowe, "Effects of Water Depth Mismatch on Matched-Field Localization in Shallow Water," *J. Acoust. Soc. Am.* **83**, 2180–2185 (1988).

[26] C. Feuillade, D. R. DelBalzo, and M. M. Rowe," Environmental Mismatch in Shallow-Water Matched-Field Processing: Geoacoustic Parameter Variability," *J. Acoust. Soc. Am.* **85**, 2354–2364 (1989).

[27] A. Tolstoy, "Sensitivity of Matched-Field Processing to Sound-Speed Profile Mismatch for Vertical Arrays in a Deep Water Pacific Environment," *J. Acoust. Soc. Am.* **85**, 2394–2404 (1989).

[28] J. M. Ozard, G. H. Brooke, and P. Brouwer, "Improving Performance for Matched-Field Processing with a Minimum Variance Beamformer," *J. Acoust. Soc. Am.* **91**, 141–150 (1992).

[29] J. R. Daugherty and J. F. Lynch, "Surface Wave, Internal Wave, and Source Motion Effects on Matched-Field Processing in a Shallow Water Waveguide," *J. Acoust. Soc. Am.* **87**, 2503–2526 (1990).

[30] A. B. Baggeroer, W. A. Kuperman, and H. Schmidt, "Matched-Field Processing: Source Localization in Correlated Noise as an Optimum Parameter Estimation Problem," *J. Acoust. Soc. Am.* **83**, 571–587 (1988).

[31] H. Schmidt, A. B. Baggeroer, W. A. Kuperman, and E. K. Scheer, "Environmentally Tolerant Beamforming for High-Resolution Matched-Field Processing: Deterministic Mismatch," *J. Acoust. Soc. Am.* **88**, 1851–1862 (1990).

[32] C. L. Byrne and A. K. Steele, "Stable Nonlinear Methods for Sensor Array Processing," *IEEE J. Oceanic Engin.* **OE-1**, 255–259 (1985).

[33] C. L. Byrne and A. K. Steele, "Sector-Focused Stability for High Resolution Array Processing," in Proc. IEEE Conf. on Acoustics, Speech and Signal Processing, April 1987, ICASSP '87, Dallas, TX, pp. 54.11.1–54.14.

[34] C. L. Byrne, R. I. Brent, C. Feuillade, and D. R. DelBalzo, "A Stable Data-Adaptive Method for Matched-Field Array Processing in Acoustic Waveguides," *J. Acoust. Soc. Am.* **87**, 2493–2502 (1990).

[35] G. M. Frichter, C. L. Byrne, and C. Feuillade, "Sector-Focused Stability Methods for Robust Source Localization in Matched-Field Processing," *J. Acoust. Soc. Am.* **88**, 2843–2851 (1990).

[36] G. B. Smith, H. A. Chandler, and C. Feuillade, "Performance Stability of High-Resolution Matched-Field Processors to Sound Speed Mismatch in a Shallow-Water Environment," *J. Acoust. Soc. Am.* **93**, 2617–2626 (1993).

[37] H. A. Chandler, C. Feuillade, and G. B. Smith, "Sector-Focused Processing for Stabilized Resolution of Multiple Acoustic Sources," *J. Acoust. Soc. Am.*, in press.

[38] F. B. Jensen and M. C. Ferla, "SNAP: The SACLANTCEN Normal-Mode Acoustic Propagation model," SACLANTCEN Memo, SM-121, 1979.

[39] J. E. Matthews, Naval Research Laboratory, Stennis Space Center, MS, private communication.